A theoretical and experimental study of the deformation of the piston-cylinder unit of a metrological pressure balance

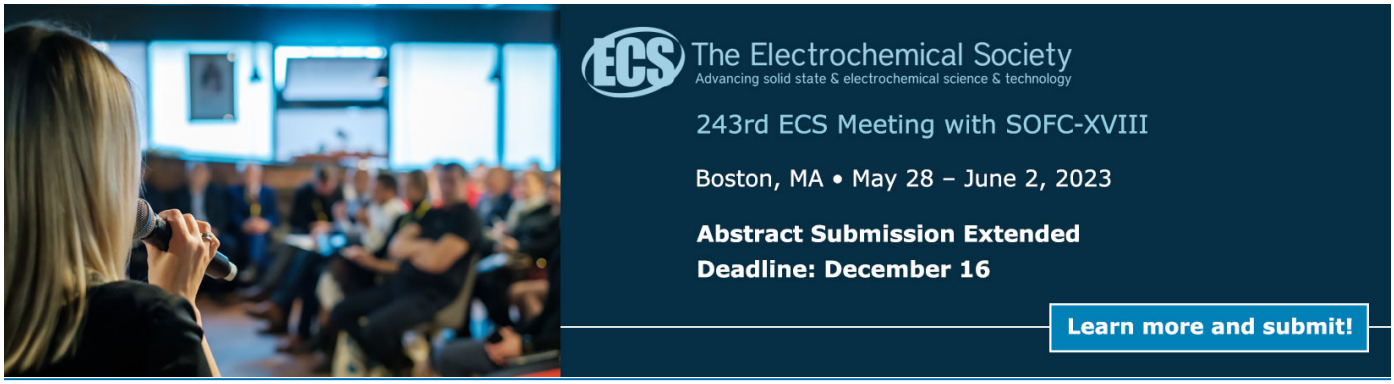

A theoretical and experimental study of the deformation of the piston-cylinder unit of a metrological pressure balance

L Soares Júnior, F I da Silva Júnior and P Lamary

Federal University of Ceará, Department of Mechanical Engineering, Fortaleza, CE, Brazil

E-mail: lsjota@gmail.com

Abstract. Pressure balance is a measuring system widely used in metrology as a reference standard. The common procedure is to estimate the pressure from an analytical formula involving a set of phenomenological parameters. These parameters are determined experimentally by calibration tests of the balance. In particular, the piston-cylinder deformation is taking into account by the use of a global distortion coefficient and by the use of an effective area of the piston. In order to analyze the possible influence of local deformation on the pressure estimation, a Finite Element (FE) model has been developed using OpenCavok FE code. For a given position of the piston in the cylinder chamber, for a given initial gap between of the cylinder and the chamber, a coupled fluid-structure calculation is carried out. From the local fields, mean values are calculated from which the effective area of the piston-cylinder unit. The analysis is conducted for several engagement lengths of the piston in the chamber and for several loads. The first results obtained show that the local deformation play a role and that FE models could help for precise calculation of the measured pressure.

1. Introduction

This paper focuses on pressure balance system used in metrology laboratories as a reference standard to measure pressure. This measurement system is also referred as dead-weight testers. Its operating principle lies in the balance, or compensation, between i) an upward force, applied on the base of the piston and defined as the multiplication of the pressure exerted by the fluid by the known cross sectional area of the piston-cylinder assembly, and ii) a downward force generated by a set of standard masses which act on the top of the balance piston under the influence of local acceleration of gravity [1, 2], as shown in figure 1.

The vertical piston of figure 1 can move freely in the cylinder chamber owing to a micro-metric gap in-between the two parts. This clearance is necessary, so that, while the piston moves, the frictional forces between the two elements are minimized avoiding a possible jamming owing to the forces generated by the action of static friction [3]. The geometry and size of the set are controlled with care and realized with high quality materials, in such a way that the effective area of the piston is determined with high accuracy. The action of the fluid on the base of the piston and on the lateral surface along the cylinder causes mechanical deformation of the assembly. An excessive leakage could alter the effective area depending of the applied pressure value.

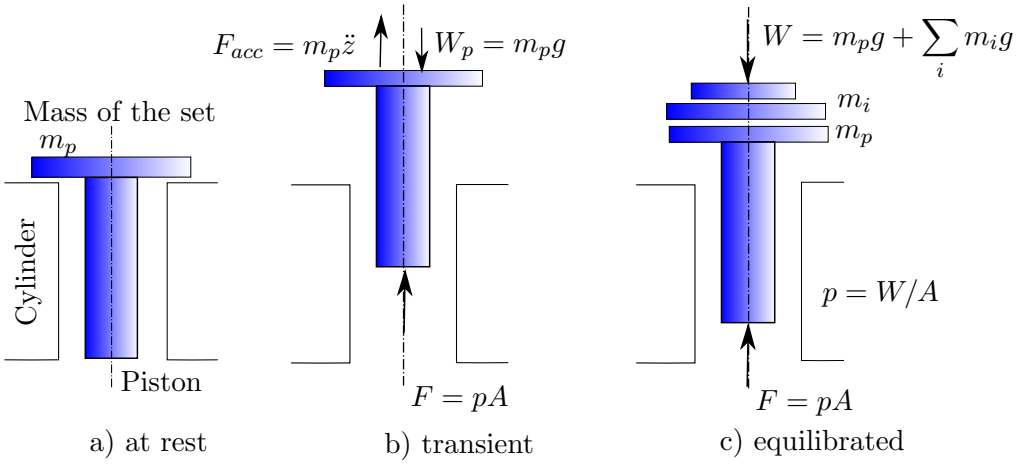

Figure 1. Pressure balance measuring principle: a) the balance is at rest, b) transient phase when the balance is put under pressure, c) disks of variable masses are put on the top of the balance as to find an equilibrated position.

The pressure measured by a balance is obtained from the analysis of the different components of the forces applied to the system. For a balance which operates with liquid, the measured pressure is given by:

$$p = \frac{\left[m_p(1 - \frac{\rho_a}{\rho_{mp}}) + m_r(1 - \frac{\rho_a}{\rho_{mr}})\right] g_l + \sigma C}{A_{0,T}\left[1 + (\alpha_c + \alpha_p)(\theta - 20)\right](1 + \lambda p_n)} \pm \rho_{fluide} g_l \Delta h \tag{1}$$

where,
p is the measured pressure, given in Pa,
m_p is the mass of the piston, in kg,
ρ_a is the specific volumetric mass of the air, in kg/m^3,
ρ_{mp} is the volumetric mass of the piston material, in kg/m^3 ,
m_r is the sum of the remaining masses operating on the system, in kg ,
ρ_{mr} is the specific volumetric mass of the remaining masses, in kg/m^3,
g_l is the acceleration due to the local gravity, in m/s^2,
σ is the surface tension of the fluid, in N/m ,
C is the length of the circumference of the piston, in m,
$A_{0,T}$ is the area of the piston cylinder assembly, in m^2,
T is the reference temperature of the piston, in ^oC ,
$\alpha_c + \alpha_p$ is the coefficient of the linear thermal expansion of the piston cylinder assembly, in $^oC^{-1}$,
θ is the temperature of the piston at the time of the measurement, in ^oC,
λ is the distortion coefficient of the piston-cylinder assembly, generally in $(10^{-6})MPa^{-1}$,
p_n is the rated pressure of the measurement given in MPa,
ρ_{fluide} is the specific volumetric mass of the fluid used, in kg/m^{-3},
Δh is the gap between the piston and the cylinder at the location where the pressure is measured, and is given in m.

A way to use equation (1) can be illustrated as follows. Be an equipment, such as a manometer, to be calibrated using the pressure balance. The manometer is connected to the balance and the procedure of figure 1 is followed, putting masses on the top of the balance as to reach the equilibrium of the piston. Next, the formula is used where p_n is the pressure indicated

by the manometer and p is the true pressure.

In equation (1), it can be seen that the variation of the effective area of the piston-cylinder assembly (the denominator of the first term) is assumed linear in regards to the applied pressure. Assuming that the temperatures at the time of the calibration of the pressure balance and at the time of the measurement of an equipment are 20^oC ($T = \theta = 20^oC$), the effective area, $A_{effective}$, may be written in the form of equation(2) as,

$$A_{effective} = A_{0,20}(1 + \lambda p_n) \tag{2}$$

The objective of this work is to study the piston-cylinder assembly behavior from the point of view of the elastic deformations. The effective area given by the phenomenological equation (2) will be compared to numerical simulation based on Finite Element Analysis (FEA). The model and the developments carried out in OpenCavok FE code are also addressed.

2. Methodology

The study was conducted considering the VEB Gertewerk oil-operated pressure balance of figure 2. It consists of piston-cylinder unit of figure 3, that can be sighted in the middle of the figure 2 with its initial mass disk on the top. At the left-side and right-side, the balance is equipped with of two vertical tubes where the equipment to be calibrated can be mounted. The balance operates in the nominal range of $[5; 50]MPa$. The hydraulic fluid is a Tellus VG 32 oil.

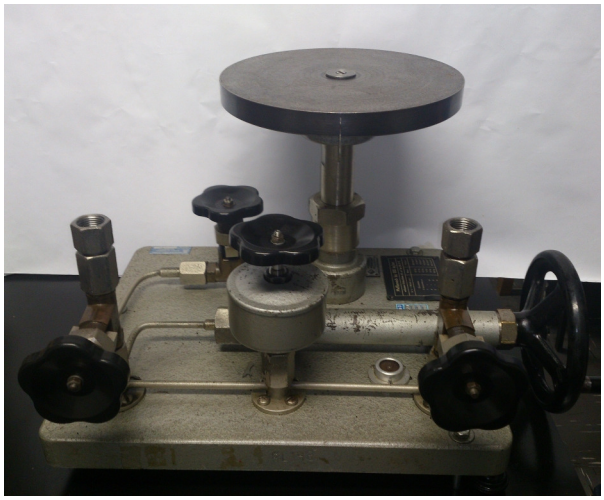

Figure 2. The VEB Gertewerk pressure balance studied.

Figure 3. The piston-cylinder assembly.

2.1. Calibration tests

The most common method of pressure balance calibration involves a comparison with a second reference pressure balance generating a known pressure. The process operates by cross-floating pressures in a closed system loop and makes the calculation of the effective area (of the balance under test) at a zero-pressure point and at standard temperature of 20^oC. The pressure distortion coefficient (λ) of the piston-cylinder assembly is also evaluated [2, 4]. Calibration tests follow a strict procedure that gives rise to calibration test reports. Five calibration tests were carried out over the past 25 years. The table 1 is extracted from these tests and recalls the values obtained for $A_{0,20}$ and λ, the two parameters involved in the formula of equation (2) under our present interest.

Table 1. Measured values of $A_{0,20}$, the area of the piston-cylinder assembly and λ, the distortion coefficient of the piston-cylinder assembly, from 5 calibration tests.

	Test 1	Test 2	Test 3	Test 4	Test 5	Units
$A_{0,20}$	9.971	9.994	9.989	9.984	9.984	$(10^{-6})m^2$
λ	—	—	-2.107	—	-2.107	$(10^{-6})MPa^{-1}$

2.2. Finite element model

A finite element model has been developed using OpenCavok FE software [5]. The Reference FE generator of OpenCavok has been extended in order to be able to define axisymmetric FEs. The related theoretical developments are given in Appendix A.

The finite element model includes two types of physical domain, i) the solid domain, comprising the piston and the cylinder, and ii) the fluid domain, comprising the fluid cavity below the piston and the gap between the cylinder and the piston. The figure 4 presents these parts. The pressure balance is axisymmetric (geometry and loads) and therefore it only needs to be modeled in the half-plane given by the axis of symmetry and a positive radial direction. Bi-dimensional structural and hydrostatic fluid elements were developed for this purpose and used. The localization of the boundary conditions can also be sighted in this picture (figure 4). The axial displacements of the cylinder at the top are restrained. The fluid, also modeled using displacement elements, is contained at the top in the axial direction. The piston is put in a given position for the calculation and restrained at the top for its axial displacement. Along the axis of symmetry, the radial displacements were fixed to ease the resolution. At the bottom, the pressure will be input using a special pressure-to-force axisymmetric mono-dimensional FE.

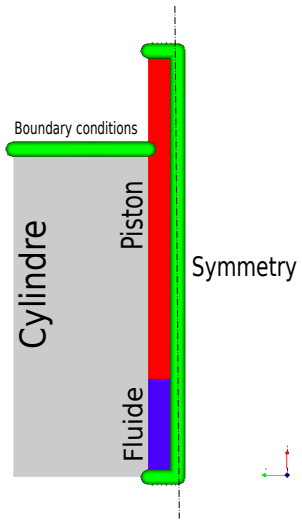

Figure 4. OpenCavokV6 axisymmetric finite element model. Main parts and boundary conditions.

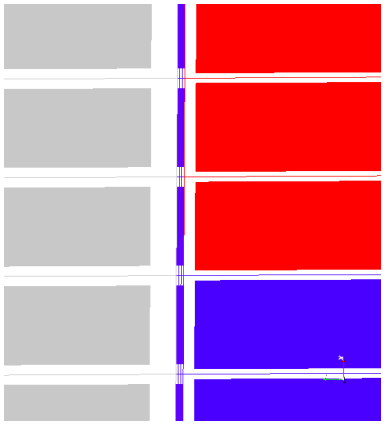

Figure 5. Zoom on the mesh at the junction of the piston (red) with the cylinder (gray). The fluid cavity (blue) and the fluid contact layer (blue) between the piston and the cylinder can be seen.

Figure 5 is a zoom on the mesh region of the interface between the piston and the cylinder.

The fluid interface is modeled by 3 fluid elements in the radial direction. The size ratio (length/thickness) of these elements is large but their strict rectangular shape should avoid numerical problems. We may note that other approaches are possible. In the research proposed by [6], the fluid is modeled using an analytical formula. The interesting point in this approach is that the fluid model includes more parameters, such as the viscosity and a net flow rate, than FE hydrostatic fluid. The FE displacements of the piston and of the cylinder are reached, in this case, by iteration.

Finally, the model consists in 280,000 finite elements. For a given pressure and a given position, the model is solved in less than 2 minutes. Calculations were carried out considering several positions of the piston and several loads. The analyses took benefit of the full parametrization capability of the FE software.

The data used are the following, the piston has a diameter of $3.5616mm$ and is made of stainless steel with an elastic modulus of $193GPa$ and a Poisson's ratio of 0.31. The cylinder is made of the same material and have a clearance with the piston of $0.003mm$ ($\phi_{cyl} - \phi_{piston}$). For the calculation were considered, a cylinder external diameter of $20mm$, a piston length of $20mm$ and a cylinder length of $20mm$. The fluid is considered incompressible and a value of $2.54(10^9)Pa$ is used for its bulk modulus.

Concerning the analytical formula of equation (2) that will serve to compare the results, the following data were used: an average effective area of $9.9712(10^{-6})m^2$ and a distortion coefficient of $2.107(10^{-12})Pa^{-1}$.

3. Results

The figures 6 and 7 illustrate the results for a given pressure of $p = 35MPa$. Figure 6 is a view of the radial displacement field of the piston-cylinder assembly for a specific engagement length (70%) of the piston in the chamber. Figure 7 is a view of the axial displacements of the piston to verify that the piston moves correctly in that direction.

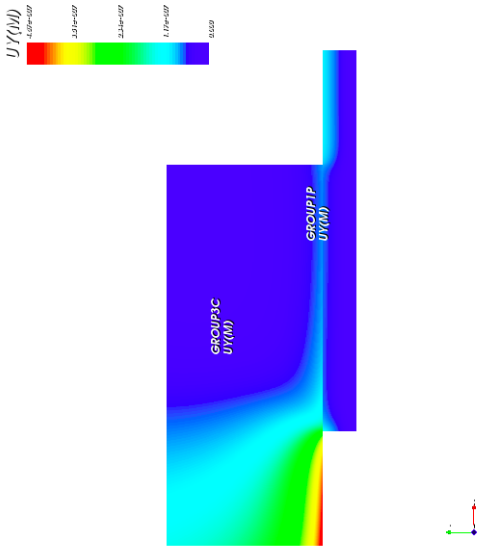

Figure 6. Radial displacements, axisymmetric model.

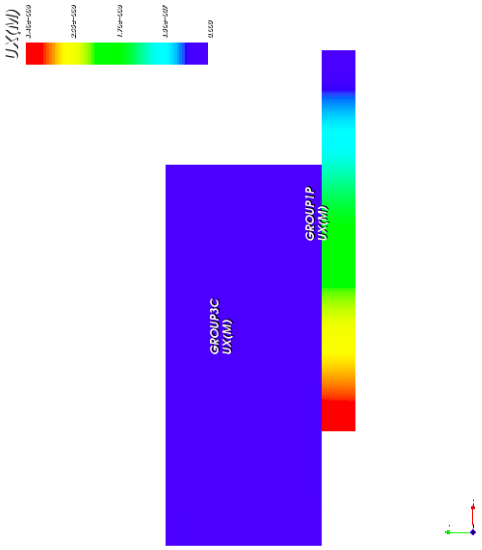

Figure 7. Axial displacements, axisymmetric model.

From the nodal displacements of the cylinder and of the piston at their interface, is computed, for each discrete position along the axis, the corresponding effective area. The mean value of

all these areas is assumed to be the effective FE area. Figure 8 presents, for a given pressure, the evolution of the effective area while considering several engagement lengths of the piston in the chamber. An engagement length of zero corresponds to the top position of the piston. The results indicate that the effective area is not constant as the engagement length changes. Figure 9 is an analysis for a given engagement length (30%) but with varying input pressure (in the $[5; 50]MPa$ range of the pressure balance). It shows that, for this given engagement length, the distortion coefficient (the slope of the curves) is higher when using FE simulation. Both curves, the analytical one, and FE one, are linear.

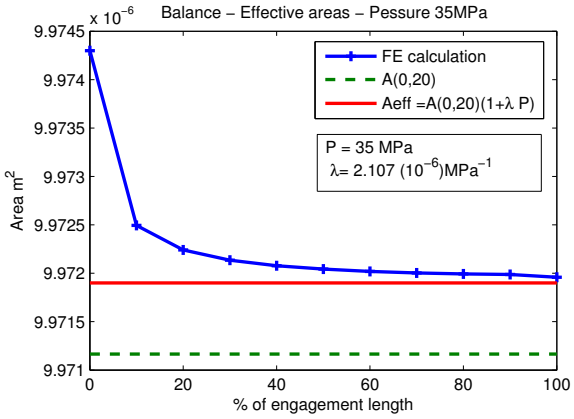

Figure 8. Effective areas as a function of the engagement length.

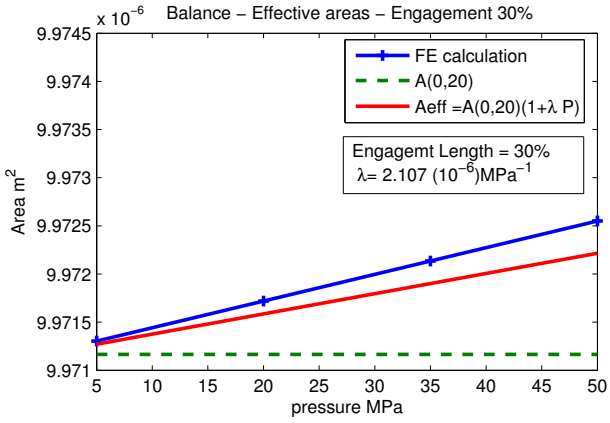

Figure 9. Effective areas as a function of the applied pressure.

4. Conclusion

Preliminary results from FEA simulations suggest a possible influence of the elastic behavior of the piston-cylinder assembly under various conditions of pressure and piston positions. It seems worthwhile to continue this investigation. From our experience, the structural parts are well-modeled by the equations and by the FE elements used. Coming efforts should concentrate themselves on the fluid models and on the boundary conditions.

Acknowledgments

The authors would like to acknowledge the CT-UFC, Center of Technology of the Federal University of Ceará, for its financial support and the group the LAMETRO-UFC, the Laboratory of Mechanical Metrology at UFC.

Appendix A. Axisymmetric FE elements

Appendix A.1. General formulation

The local equilibrium, for any point, $\mathcal{P}$, of the solid domain, $\mathcal{D}$, can be written as the divergence of the stress tensor, $\overline{\overline{\sigma}}(\vec{u})$, $\vec{u}$ being the displacement vector, in the following form,

$$\vec{div}(\overline{\overline{\sigma}}(\vec{u})) = \vec{0} \quad \forall \mathcal{P} \in \mathcal{D} \tag{A.1}$$

The frontier $\partial\mathcal{D}$ of $\mathcal{D}$ can be shared into two parts, $\partial\mathcal{D} = \partial\mathcal{D}_u \bigcup \partial\mathcal{D}_T$, with $\partial\mathcal{D}_u$ a frontier where the $\vec{u}$ is known, and, $\partial\mathcal{D}_T$ a frontier where the normal stress vector is known. We may write these boundary conditions as,

$$\left\{ \begin{array}{rcll} \vec{u} & = & \vec{u_d} & \forall \mathcal{P} \in \partial \mathcal{D}_u \\ \overline{\overline{\sigma}}\vec{n} & = & \vec{T_d} & \forall \mathcal{P} \in \partial \mathcal{D}_T \end{array} \right. \tag{A.2}$$

Following the finite element method, a test function, $\vec{P}$, is introduced and the equation (A.1) is rewritten into an integral form, W, as,

$$W = \int_{\mathcal{D}} \vec{P}.\vec{div}(\overline{\overline{\sigma}})dV = 0 \quad \forall \vec{P} \quad \text{kinematically admissible} \tag{A.3}$$

Using the identity formula of equation (A.4), equation (A.3) is rewritten as equation (A.5) which allows the use of the Ostrogadsky theorem formula given in equation (A.6) to establish a weak form of W as stated by equation (A.7).

$$\overline{\overline{\sigma}} : \overline{\overline{grad_s}}(\vec{P}) = div(\overline{\overline{\sigma}}\vec{P}) - \vec{P}.\vec{div}(\overline{\overline{\sigma}}) \tag{A.4}$$

$$W = \int_{\mathcal{D}} (\overline{\overline{\sigma}} : \overline{\overline{grad_s}}(\vec{P}) - div(\overline{\overline{\sigma}}\vec{P}))dV = 0 \tag{A.5}$$

$$\int_{\mathcal{D}} div(\overline{\overline{\sigma}}\vec{P})dV = \int_{\partial \mathcal{D}} \overline{\overline{\sigma}}\vec{P}.\vec{n}dS = \int_{\partial \mathcal{D}} \vec{P}.\overline{\overline{\sigma}}\vec{n}dS \tag{A.6}$$

$$W_{weak} = \int_{\mathcal{D}} \overline{\overline{\sigma}} : \overline{\overline{grad_s}}(\vec{P})dV - \int_{\partial \mathcal{D}} \vec{P}.\overline{\overline{\sigma}}\vec{n}dS = 0 \tag{A.7}$$

Choosing, among all the kinematically admissible test functions $\vec{P}$, the functions which take a null value on $\partial \mathcal{D}_u$ and applying the known values $\vec{T_d}$ on $\partial \mathcal{D}_T$, the final form of the weak variational integral is,

$$W_{weak} = \int_{\mathcal{D}} \overline{\overline{\sigma}} : \overline{\overline{grad_s}}(\vec{P})dV - \int_{\partial \mathcal{D}_\mathcal{T}} \vec{P}.\vec{T_d}dS = 0 \tag{A.8}$$

Putting the unknowns, $\vec{u}$, on the left-hand side and the known loads, $\vec{T_d}$, on the right-hand side, the equation (A.8) becomes,

$$\int_{\mathcal{D}} \overline{\overline{\sigma}}(\vec{u}) : \overline{\overline{grad_s}}(\vec{P})dV = \int_{\partial \mathcal{D}_\mathcal{T}} \vec{P}.\vec{T_d}dS \tag{A.9}$$

Following the Galerkine method, the test functions $\vec{P}$ are chosen as virtual displacements that we may note as $\vec{P} = \delta\vec{u}$, leading therefore to the following equation,

$$\int_{\mathcal{D}} \overline{\overline{\sigma}}(\vec{u}) : \delta\overline{\overline{\epsilon}}(\delta\vec{u})dV = \int_{\partial \mathcal{D}_\mathcal{T}} \delta\vec{u}.\vec{T_d}dS \quad \forall \delta\vec{u} \quad \text{kinematically admissible} \tag{A.10}$$

where $\delta\overline{\overline{\epsilon}}$ is the strain tensor due to the virtual displacements $\delta\vec{u}$.

Appendix A.2. Axisymmetric formulation

For axisymmetric solids, in regards to the geometry and to the applied loads, it is assumed that there is no displacement in the circumferential direction. The integrals of equation (A.10) are transformed into a cylindric coordinates system (ρ, θ, z) from which the elementary volume dV expressed as $dV = \rho d\rho d\theta dz$. Equation (A.10) becomes,

$$2\pi \int_{\mathcal{P}^+} \rho(\overline{\overline{\sigma}}(\vec{u}) : \delta\overline{\overline{\epsilon}}(\delta\vec{u}))d\rho dz = 2\pi \int_{\partial \mathcal{P}^+} \rho(\delta\vec{u}.\vec{T_d})dl \quad \forall \delta\vec{u} \quad \text{kinematically admissible} \tag{A.11}$$

where,
$\mathcal{P}^+$ is the 2D domain of the solid when cut by the plane (ρ, z) for ρ positive,
$\partial\mathcal{P}^+$ is the oriented contour of this domain from which dl is an infinitesimal element,
All the entities, the tensors and the vectors, have now to be expressed in the cylindrical coordinates system. Which is done using classical formulae.

The domain $\mathcal{P}^+$ is discretized using bi-dimensional finite elements, the domain $\partial\mathcal{P}^+$, if needed, is discretized using mono-dimensional finite elements. Linear approximations were used. The calculus of the integral can now be done as the sum of all the elementary integrals. These are evaluated numerically using the approximation functions and evaluating also ρ at each gauss point. Equation (A.11) takes the following discrete form,

$$2\pi\delta\vec{U}.([K]\vec{U}) = 2\pi\delta\vec{U}.\vec{F} \quad \forall\delta\vec{U} \quad \text{kinematically admissible} \tag{A.12}$$

where,
$\vec{U}$ accounts for the discretized nodal displacements,
$\delta\vec{U}$ accounts for the discretized virtual nodal displacements,
$[K]$ accounts for the global stiffness matrix,
$\vec{F}$ accounts for the applied nodal loads.

As the equation is valid, $\forall\delta\vec{U}$, the algebraic system of equation (A.13) is equivalent to equation (A.12). This system will be solved by the Finite Element solver, introducing, at that time, the kinematic boundaries conditions.

$$[K]\vec{U} = \vec{F} \tag{A.13}$$

Appendix A.3. Fluid-structure coupling
For the present work, we considered that the fluid is contained and that there is no net flow rate. The fluid can be modeled using the same approach as for the structural elements, with displacements as main unknowns. The physical components of stress-strain tensors are adapted using the bulk modulus of the fluid. The viscosity could be introduced, to compute a damping matrix, in the case of dynamic analyses.

Introducing the subscript s for the solid and f for the fluid, the coupled system of equations can be written as,

$$\begin{cases} [K_s]\vec{U_s} &= \vec{F_s} \\ [K_f]\vec{U_f} &= \vec{F_f} \end{cases} \tag{A.14}$$

As the structural parts and the fluid part are modeled using the same types of unknowns (displacements), the coupling is automatic when structural and fluid elements are in contact at a given node. The stiffness terms coming both from the structure and the fluid are added. In the second member of equation (A.14), the structural loads coming from the action of the fluid on the structure are automatically equilibrated by the fluid loads coming from the action of the structure on the fluid and the sum of these components vanish. Finally, a system of the form of equation (A.15) has to be solved.

$$[K]\vec{U} = \vec{F} \tag{A.15}$$

References

[1] Dadson R S, Lewis S L and Peggs G N 1982 *The Pressure Balance: Theory and Practice* (London: H.M.S.O.)
[2] Dadson R S, Lewis S L and Peggs G N 2011 *Calibration of Pressure Balances* (EURAMET cg-3)

[3] Lewis S L and Peggs G N 1992 *The Pressure Balance: A Practical Guide to Its Use* (London: H.M.S.O.)
[4] Kobata T 2011 Multiple cross-float system for calibrating pressure balances *Proc. of the 5th CCM and 4th IMEKO TC16* (Berlin)
[5] Lamary P, de Araujo Bezerra R, da Silva Junior F I, Pontes de Deus E and Benallal A 2014 A multi-physic implementation of the finite element method apllied to research on acoustic poro-elastic materials *Proc. of the CILAMCE* (Fortaleza) DOI: 10.13140/2.1.3301.6644
[6] Yagmura L and Bagli E F 2009 Experimental and dimensional characterization of a prototype piston-cylinder unit and validation using finite element analysis (FEA) *Measurement* B **42** 678-684